# An exploratory assessment of early and delta PET radiomic features for outcome prediction in locally advanced cervical cancer

Florit, A.; Noortman, W.A.; Bizzarri, N.; Pasciuto, T.; Feudo, V.; Annunziata, S.; ... ; Collarino, A.

European Journal of Nuclear Medicine and Molecular Imaging
https://doi.org/10.1007/s00259-025-07405-w

ORIGINAL ARTICLE

# An exploratory assessment of early and delta PET radiomic features for outcome prediction in locally advanced cervical cancer

Anita Florit[1,2] · Wyanne A. Noortman[3] · Nicolò Bizzarri[4] · Tina Pasciuto[5,6] · Vanessa Feudo[7] · Salvatore Annunziata[1] · Lioe-Fee de Geus-Oei[2,8,9] · Elisabeth Pfaehler[10] · Ronald Boellaard[11] · Maria Antonietta Gambacorta[12,13] · Gian Franco Zannoni[14,15] · Gabriella Ferrandina[4,16] · Evis Sala[13,17] · Giovanni Scambia[4,16] · Vittoria Rufini[1,7] · Floris H. P. van Velden[8] · Angela Collarino[1]

Received: 13 February 2025 / Accepted: 5 June 2025


## Abstract

**Purpose** This study investigated whether radiomic features extracted from [$^{18}$F]FDG-PET scans acquired before and two weeks after neoadjuvant treatment, and their variation, provided prognostic parameters in locally advanced cervical cancer (LACC) patients treated with neoadjuvant chemo-radiotherapy (CRT) followed by radical surgery.

**Methods** We retrospectively included LACC patients referred to our Institution from 2010 to 2016. [$^{18}$F]FDG-PET/CT was performed before neoadjuvant CRT (baseline) and two weeks after the start of treatment (early). Radiomic features were extracted after semi-automatic delineation of the primary tumour, on baseline and early PET images. Delta radiomics were calculated as the relative differences between baseline and early features. We performed 5-fold cross-validation stratified for recurrence and cancer-specific death, integrating dimensionality reduction of the radiomic features and variable hunting with importance within the folds. After supervised feature selection, radiomic models with the best-performing features for each timepoint, as well as clinical models and combined clinico-radiomic models, were built. Model performances are presented as C-indices, for prediction of recurrence/progression (disease-free survival, DFS) and cancer-specific death (overall survival, OS).

**Results** 95 patients were included. With a median follow-up of 76.0 months (95% CI: 59.5–82.1), 31.6% of patients had recurrence/progression and 20.0% died of disease. None of the models could predict DFS (C-indices $\leq$ 0.72). Model performances for OS yielded slightly better results, with mean C-indices of 0.75 for both the radiomic and combined model based on early features, 0.79 and 0.78 for the radiomic and combined model derived from delta features, and 0.76 for the clinical models.

**Conclusion** [$^{18}$F]FDG-PET early and delta radiomic features could not predict DFS in patients with LACC treated with neoadjuvant CRT followed by radical surgery. Although slightly improved performances for the radiomic and combined models were observed in the prediction of OS compared to the clinical model, the added value of these parameters and their inclusion in the clinical practice seems to be limited.

**Keywords** Locally advanced cervical cancer · [$^{18}$F]FDG-PET/CT · Delta radiomics · Prognosis

## Introduction

The standard treatment for locally advanced cervical cancer (LACC, 2018 FIGO stages IB3-IVA) is pelvic external-beam radiotherapy, with concurrent platinum-containing chemotherapy (CRT) and brachytherapy [1]. However, almost one third of LACC patients will experience recurrence within 2 years after exclusive CRT [2, 3]. An alternative strategy is completion surgery following neoadjuvant CRT, aimed at removing residual tumour resistant to CRT, which has shown survival rates comparable to the standard approach [4]. Regardless of the treatment protocol adopted,

Floris H. P. van Velden and Angela Collarino share last authorship.

Extended author information available on the last page of the article

Published online: 18 June 2025

in the view of a more personalised medicine, it is relevant to early identify non-responding or early recurring patients to optimise treatment protocols and predict survival.

In the last few years, several studies have investigated the extraction and analysis of various advanced quantitative characteristics (features) from biomedical images. This approach, denoted as radiomics, has been applied to positron emission tomography/computed tomography (PET/CT) imaging as well, to define tumour characteristics related to intensity, shape, and texture (i.e., intratumour heterogeneity). These features have shown promising results in the prediction of treatment response, survival and in differentiating benign and malignant tumours [5, 6].

To date, several studies have explored PET-derived radiomic features in patients with LACC [7–20], namely when the tumour has grown beyond the cervix and uterus, and it might have spread to other organs in the pelvic region (e.g., vagina, bladder and/or rectum) and loco-regional lymph nodes [21]. Most of the literature on this topic explored the correlation of the features derived from pretreatment PET scans with treatment response [7–9] and prognosis [10–20], with mixed results. Our previous study on a large cohort of LACC patients showed that pretreatment 2-deoxy-2-[$^{18}$F]fluoro-D-glucose ([$^{18}$F]FDG)-PET radiomic features could not predict histopathologic tumour response and survival [22]. So far, few studies (including a total of 64 patients) have explored the correlation of the temporal variation of the radiomic features (denoted as "delta radiomics"), extracted from PET acquired at different timepoints, with response to therapy and survival in LACC patients treated with exclusive CRT [7, 9]. The rationale is that early prediction of treatment outcome might offer an opportunity to identify non-responding or early recurring patients and promptly modify the therapy, for example by intensifying the treatment scheme or performing completion hysterectomy. We hypothesised that variations in intratumoural metabolic parameters during treatment may early reflect tumour response to CRT, providing valuable insights into patients' prognosis. Therefore, this exploratory study aimed to assess whether features derived from [$^{18}$F]FDG-PET studies acquired two weeks after neoadjuvant treatment ("early") and their variation from the baseline scan ("delta") could correlate with prognosis in LACC patients treated with neoadjuvant CRT followed by radical surgery.

## Materials and methods

### Patients and study design

In this retrospective study, medical records of all consecutive LACC patients, which were referred to the Gynaecologic Oncology Unit at the Fondazione Policlinico Universitario A. Gemelli IRCCS between July 2010 and July 2016, were reviewed. This study was approved by the Ethical Committee of the Fondazione Policlinico Universitario A. Gemelli IRCCS (study code 3860). Patients were included if they were at least 18 years old, underwent [$^{18}$F]FDG-PET/CT scans before treatment ("baseline" imaging) and two weeks after the start of neoadjuvant CRT ("early" imaging), completed their treatment with CRT followed by surgery and were monitored with follow-up. Early PET/CT was acquired after two weeks of treatment, as radiation-induced inflammation was expected to be minimal at this stage.

Patients were not eligible if they had distant metastatic disease, prior loco-regional surgery, chemotherapy, or loco-regional radiation therapy within 5 years before inclusion. Written informed consent was obtained from all patients. Clinical data were extracted from the patient medical records and collected using the Research Electronic Data Capture (REDCap) tool hosted at Fondazione Policlinico Universitario A. Gemelli IRCCS [23].

### Treatment and follow-up

All patients were treated with neoadjuvant CRT, as described by Ferrandina et al. [24]. The treatment scheme is presented in Fig. 1. Following neoadjuvant therapy, each patient underwent radical hysterectomy and pelvic, with or without aortic, lymphadenectomy. Histopathological evaluation was performed by an experienced gynaecologic oncologist pathologist (G.F.Z.). Pathological disease response was defined as complete (absence of any residual tumour after

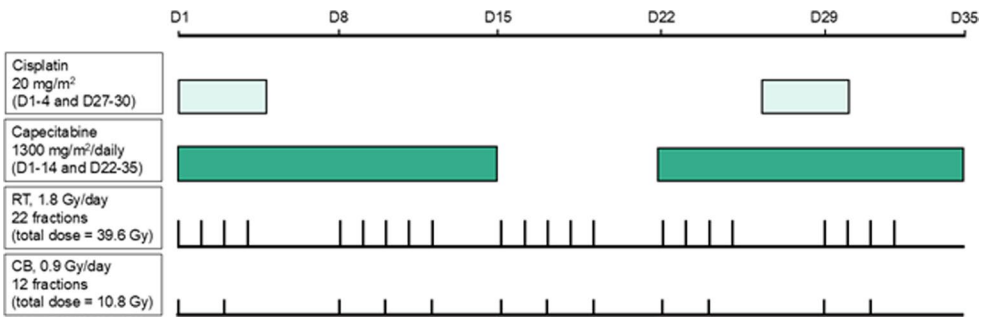


**Fig. 1** Concomitant chemoradiotherapy scheme. CB: Concomitant boosts to the primary tumour and parametria. D: Day. RT: Conformal irradiation of the bulky tumour, pelvic lymph nodes drainage, and parametria

treatment at any site level, pR0), or partial, including microscopic (persistent tumour foci ≤ 3 mm maximum dimension, pR1), and macroscopic (persistent tumour foci > 3 mm maximum dimension, pR2) residual tumour [25].

Clinical follow-up consisted of history and physical examination every 3 months for 2 years, every 6 months for other 3 years and then annually based on patient risk of disease recurrence. Patients underwent ultrasound and magnetic resonance every 6 months plus chest-abdomen CT annually, for 2 years [1]. Recurrence/progression was confirmed through biopsy or follow-up imaging. Vaginal and/or cervical recurrence/progression was classified as local, pelvic/para-aortic as regional, and upper abdominal and/or extra-abdominal as distant [1].

## PET/CT image acquisition and reconstruction

Baseline and early PET/CT scans were performed as previously described [26]. Images were acquired at a mean time of 65 ± 8 min after intravenous administration of [$^{18}$F]FDG on a Gemini GXL (Philips Healthcare, Best, The Netherlands) or a Biograph mCT (Siemens Healthineers, Erlangen, Germany) PET/CT scanner [27]. A low-dose CT scan (110–120 kV, 40–50 mAs) was acquired from the skull to the pelvis for anatomic reference and attenuation correction purposes. The PET scans were obtained in the same anatomical range, with imaging times of 2.5–3.0 min per bed position. All PET images were reconstructed according to the recommended settings set by the European Association of Nuclear Medicine (EANM) Research Ltd. (EARL) $^{18}$F standard 1 [28], using either a line-of-response row-action maximum-likelihood algorithm (3 iterations and 33 subsets, voxel size of 4 × 4 × 4 mm, no additional Gaussian smoothing) or a 3-dimensional (3D) ordered-subsets expectation-maximization algorithm with resolution modelling (2 iterations and 21 subsets, voxel size of 3.2 × 3.2 × 5 mm, additional Gaussian smoothing of 8 mm full-width-at-half-maximum) for the Gemini or Biograph, respectively.

## Radiomic analysis

### Segmentation

PET/CT image analysis and tumour segmentation were performed by a nuclear medicine physicians (A.F.) and the results were checked by a second nuclear medicine physician (A.C.). In case of disagreement, the decision was made by consensus. The two nuclear medicine physicians were blinded to the clinical, histopathological and follow-up information. Primary tumour volumes were segmented on baseline and early PET images using the ACCURATE tool [29]. The volumes of interest (VOIs) were drawn semiautomatically with an isocontour method that applies a threshold of 50% of the body-weighted peak standardized uptake value ($SUV_{peak}$) corrected for local background activity [30, 31]. $SUV_{peak}$ was defined as the highest mean SUV ($SUV_{mean}$) of a 1 mL sphere within the VOI. Areas of physiological high [$^{18}$F]FDG uptake close to the primary tumour (e.g., bladder, ureters) were manually excluded when needed.

### Image processing and feature extraction

Five conventional PET features (i.e., $SUV_{peak}$; $SUV_{mean}$; maximum SUV [$SUV_{max}$]; total lesion glycolysis and metabolic tumour volume) were extracted from the original VOIs. Prior to radiomic feature calculation, all PET images were resampled to a voxel size of 2 × 2 × 2 mm$^3$ using trilinear interpolation and their grey levels were discretized applying a fixed bin size of 0.25 SUV [32].

A total of 166 radiomic features was extracted from both baseline and early PET scans using RaCaT v.1.28 [33], based on shape ($n$ = 22), local intensity ($n$ = 2), intensity volume histograms ($n$ = 6), intensity histograms ($n$ = 24), first-order statistics ($n$ = 18) or texture ($n$ = 94). Textures were computed in a single matrix, including the whole volume (3D), and considering all 13 orientations simultaneously (merging strategy). Textural features were derived from the following matrices: grey-level co-occurrence matrix (GLCM, $n$ = 25), grey-level run-length matrix (GLRLM, $n$ = 16), grey-level size zone matrix (GLSZM, $n$ = 16), grey-level distance zone matrix (GLDZM, $n$ = 16), neighbourhood-grey-tone difference matrix (NGTDM, $n$ = 5) and neighbourhood-grey-level dependence matrix (NGLDM, $n$ = 16). All features were implemented according to the definitions set by the Image Biomarker Standardization Initiative (IBSI) [34].

In addition, "delta" radiomics expressing the relative differences between baseline and early features were calculated as follows [35]:

$$\Delta\, feature = \frac{feature_{early} - feature_{baseline}}{feature_{baseline}}$$

## Statistical analysis

We planned the enrolment period between July 2010 and July 2016 to ensure a minimum follow-up of 3 years necessary for survival analysis. Considering the primary objective of evaluating the feasibility of measuring radiomic features of [$^{18}$F]FDG-PET/CT scan acquired 2 weeks ± 3 days after the start of neoadjuvant CRT (early examination), and assuming a proportion of feasible patients of 70% in a 3 years study-period, a sample size of 100 examinations was

appropriate to detect the assumed proportion with a margin of error of 9.

Patient clinical characteristics included age at diagnosis, FIGO stage (according to the 2009 classification), histotype, tumour grade (G1, G2, G3), pathological disease response after surgery and pelvic nodal involvement. Patient characteristics were presented as n (%), and median (range) where appropriate. Survival prediction was performed using Cox regression analysis provided both in terms of disease-free survival (DFS) and overall survival (OS) [36]. DFS was defined as the time interval between the date of diagnosis (cervical biopsy) and the date of the first clinical or imaging detection of recurrence/progression or last follow-up. OS was defined as the time interval between the date of first diagnosis and the time when cancer-specific death occurred or last follow-up. Censoring was applied for patients lost at follow-up or dead for other causes. Median follow-up was calculated with the inverse Kaplan-Meier method.

Stratified five-fold Cox regression was performed in R version 4.4.3 (R Foundation for Statistical Computing) [37]. The dataset was split into five equal-sized folds, stratified for recurrence and cancer-specific death. Each subgroup consecutively served as a test set and the remaining four-fifths of patients served as the training set.

Dimensionality reduction of the radiomic features (divided in two timepoints, baseline and early, and delta) was incorporated in the folds, using redundancy filtering in FMradio (Factor Modelling for Radiomics Data) R-package version 1.1.1 [38] and variable hunting with variable importance (VH-VIMP) in randomForestSRC, R-package version 3.3.3 [39]. Features were normalized (centred around 0, with a variance of 1) to prevent that those with the largest scale would dominate the analysis. To reduce the high dimensionality and collinearity of the scaled feature dataset, redundancy filtering on the Spearman correlation matrix was performed (threshold for correlation was set to 0.8). Subsequently, supervised feature selection was performed using VH-VIMP, a variable selection method based on a random forest algorithm that was considered the best performing feature selection method for single-modality radiomic studies [39, 40]. This process was repeated 1,000 times, selecting a medium conservativeness, which set the number of trees to 500, the number of randomly sampled variables to determine an optimal split was set to 33% of the total number of features, and the node size was set to 2. In each of the five folds, the top ranked features in terms of occurrence were selected. A Cox proportional hazards regression model using the selected radiomic features was fitted on the training folds and validated in the test folds. In addition, a clinical model based on the two best-performing clinical characteristics, and a clinico-radiomic model that combined the radiomic features and the clinical variables, were fitted. Due to the multicollinear nature of the radiomic feature set, multiple (non or partly overlapping) sets of features were selected in the different folds (overview in Online Resource 1). Therefore, the final models and regression coefficients were based on the totality of the data (Online Resource 2). Model performances are expressed by Harrell's concordance index (C-index), a measure for the global evaluation of prognostic models in survival analysis, that takes into account both outcome occurrence and timing [41]. To assess the uniqueness of the selected features per imaging timepoint, the relation between the selected radiomic features for each timepoint and the features extracted from the other two timepoints was analysed through Spearman correlation analysis. Correlation matrices and maximum absolute correlations were presented. Finally, calibration curves, to assess calibration of the obtained models, and stratified Kaplan-Meier survival curves, illustrating DFS and OS based on the radiomic, clinical, and combined models, developed at baseline, early, and delta evaluations, were generated. Patients were stratified into high-risk and low-risk groups based on their predicted risk scores, with the median risk score serving as threshold. Survival differences between groups were assessed using the log-rank test. All estimates were provided using 95% confidence interval. Statistical analysis and plots were performed using R version 4.4.3 [37].

## Results

After reviewing 100 medical records of women with LACC submitted to neoadjuvant CRT, 95 patients were included (Fig. 2; Table 1). The majority of patients had FIGO 2009 stage IIB (72.6%) and presented histological grading G2 (56/87 patients, 64.4%). The most frequent histotype was squamous cell carcinoma (88.4%). At pathological evaluation after surgery, half of the patients had pR0 in the cervix (49.4%), the remaining half was equally divided between pR1 (25.3%) and pR2 (25.3%). Most patients (88.4%) had negative pelvic and para-aortic nodal histology, when analysed. With a median follow-up of 76.0 months (95% CI 59.5–82.1), 30 (31.6%) patients experienced recurrence/progression and 19 (20.0%) died of cervical cancer. One patient died from other causes (myocardial infarction) 31 months after cervical cancer diagnosis.

Most PET/CT images were acquired on Gemini GXL: 86/95 (90.5%) patients for baseline and 90/95 (94.7%) for early imaging; 83/95 (87.3%) underwent both scans on Gemini GXL. VOIs were drawn semiautomatically in all patients; manual correction of the VOI after semiautomatic delineation was applied on 62 PET images (32.6%) to remove areas of physiological high [$^{18}$F]FDG activity

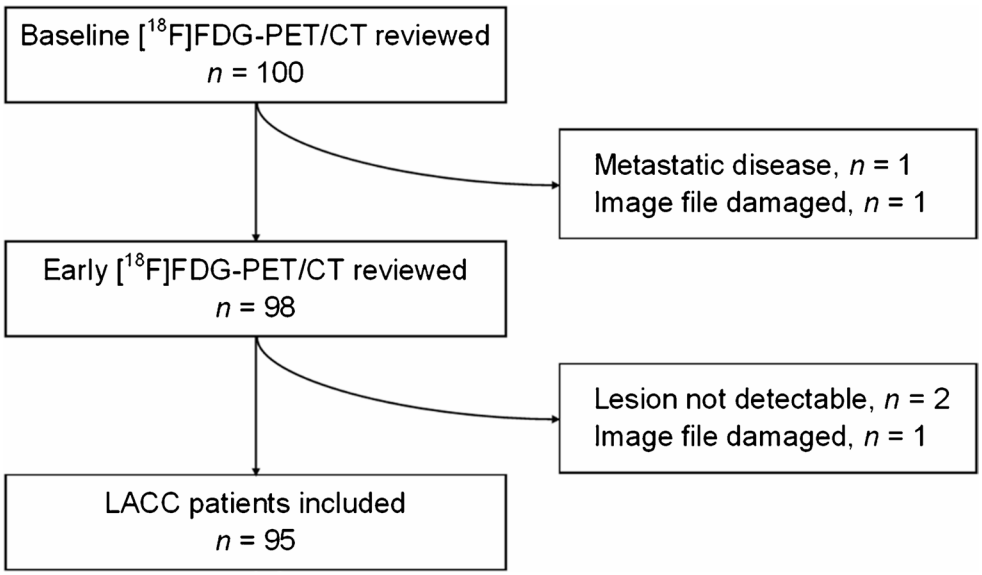


**Fig. 2** Flowchart of study population. [$^{18}$F]FDG-PET/CT: 2-deoxy-2-[$^{18}$F]fluoro-D-glucose positron emission tomography/computed tomography. LACC: Locally advanced cervical cancer

(mainly urinary) contiguous to the primary tumour. Figures 3 and 4 show PET/CT images obtained at baseline and early evaluation in two illustrative cases.

Table 2 reports model performances for the two timepoints and delta, as the mean of the C-indices (and their 95% confidence intervals) over the 5-folds, for prediction of recurrence/progression (DFS) and cancer-specific death (OS) in the testing cohorts. Detailed information about the model performances in the training cohorts can be found in the Online Resource 3. Online Resource 4 provides a graphical representation of the C-index and the corresponding 95% confidence intervals across the folds for both the training and test sets. For prediction of DFS, at the two timepoints and the delta between them, the radiomic and the combined models performed equal to or worse than the clinical model, with mean C-indices $\leq 0.72$ in the test sets. When evaluating the predictive performances of the models for OS, at baseline the clinical and the combined model performed similarly (mean C-indices of 0.76), while the radiomic model alone showed poor performances with a C-index of 0.57. The radiomic and the combined models based on delta features performed slightly better than the clinical model alone, yielding a C-index of 0.79 and 0.78 respectively, versus 0.76 (clinical model). The selected features for the radiomic models are presented in Table 3. The selected clinical characteristics for both outcomes were pathological disease response and pelvic nodal involvement. Figure 5 presents the uniqueness of the selected radiomic features for each timepoint compared to all features from other timepoints. Calibration curves plotted for the radiomic, clinical, and combined models, showed poor agreement between predicted and observed DFS and OS at 60 months, suggesting that the models overestimate the observed survival (Online Resource 5). Although the Kaplan-Meier survival curves developed at early and delta timepoints showed statistically significant difference between risk groups for the radiomic, clinical and combined models, these results offer limited additional information given the comparable prognostic performances across models in terms of C-indices (Online Resource 6).

## Discussion

In this study, we aimed to assess whether a radiomic model based on [$^{18}$F]FDG-PET features extracted from baseline and early scans, and their temporal variation, could predict DFS and OS in LACC patients treated by neoadjuvant CRT followed by surgery. Three models (radiomic, clinical and combined) were developed, and their performances were internally validated with a stratified 5-fold cross-validation. Our results showed that both the radiomic and the combined model performed similarly or worse than the clinical model in predicting recurrence or progression, while slightly improved performances for the radiomic and combined models were observed in the prediction of cancer-specific death. Based on our findings, PET radiomics derived from early scans, and their changes from baseline, do not provide additional prognostic value in LACC patients and therefore do not warrant the economic and logistical burden of an additional scan.

The predictive performance of the models in the training set were moderately good: the radiomic and the combined model achieved the best performances for the prediction of the OS at early and delta timepoints. However, when testing the radiomic and combined models, especially for the prediction of recurrence/progression, the average performance was $\leq 0.72$. These results could be related to a problem of

**Table 1** Clinical and pathological characteristics of the study population

| Characteristic | All cases ($n = 95$) |
|---|---|
| Age at diagnosis (years) | 50 (22–75) |
| Histotype | |
| Squamous cell carcinoma | 84 (88.4%) |
| Adenocarcinoma | 10 (10.5%) |
| Other | 1 (1.1%) |
| Clinical 2009 FIGO stage | |
| IB2 | 3 (3.2%) |
| IIA | 9 (9.5%) |
| IIB | 69 (72.6%) |
| IIIA | 4 (4.2%) |
| IIIB | 10 (10.5%) |
| Tumour grade† | |
| G1 | 4/87 (4.6%) |
| G2 | 56/87 (64.4%) |
| G3 | 27/87 (31.0%) |
| Pathological response | |
| Complete response | 47 (49.4%) |
| pR1 (≤ 3 mm) | 24 (25.3%) |
| pR2 (> 3 mm) | 24 (25.3%) |
| Histology of pelvic lymph nodes | |
| Negative | 84 (88.4%) |
| Positive | 11 (11.6%) |
| Median maximum tumour diameter on baseline MRI (cm) | 4.8 (1.0–11.5) |
| Median maximum tumour diameter on early MRI (cm) | 3.2 (0.8–6.2) |
| Median follow-up (months) (95% CI) | 76.0 (59.5–82.1) |
| Recurrence/progression | 30 (31.6%) |
| Cancer-specific death | 19 (20.0%) |

Results are presented as n (%) for categorical characteristics and as median (range) for continuous characteristics. *FIGO* International Federation of Gynecology and Obstetrics. † Information available for 87/95 patients. *pR* pathological response. *MRI* magnetic resonance imaging. *CI* confidence interval

overfitting of the models to the training data, which might be due to the relatively small number of patients and to an unbalanced representation of the outcomes, as well as an uneven distribution of the events across the two scanners. Regarding the unbalanced representation of the outcomes, data resampling methods were not applied to the training set, since only minimal improvement of the predictive performance of the radiomic models are expected [42]. We intend to overcome these issues by prospectively validating these models in a larger population of patients, ideally in an external clinical centre; in particular, future studies should focus on a more balanced use of different scanners.

We observed that mainly shape features were selected in the radiomic models. These features describe the geometric characteristics of the VOI, such as the major, minor (second large axis) and least axis of the volume, asphericity, and two measures of spatial autocorrelation, Geary's C and Moran's I [34]. One plausible explanation could be that after the beginning of the CRT, dimensional changes of the primary tumour are expected in patients who respond to treatment, consequently affecting their survival. Another hypothesis could be that textural features, which reflect the lesion heterogeneity, were selected less frequently than shape features because they are highly influenced by the size of the tumour, especially when they are extracted from small volumes. This especially applies to PET imaging, where intrinsic factors such as low spatial resolution and partial volume effect hinder an accurate representation of the underlying tumour heterogeneity [32, 43]. In our study, we observed smaller volumes in the early scans compared to the baseline, which may have affected the texture analysis at the second timepoint. Specifically, 28 patients had a primary tumour with maximum diameter below 2.6 cm on magnetic resonance imaging—a threshold that could impact the results of the texture analysis [44]. However, we chose to include these patients to avoid introducing bias, as these patients exhibited the best response to neoadjuvant chemotherapy. To overcome this limitation, we included only textures calculated from a single matrix that takes into account all 13 directions simultaneously, in order to retain more information, minimize the influence of noise and better represent the complexity of the distribution of grey levels [44]. It is also worth noting that PET metrics are slightly influenced by patient's position during the two acquisitions (baseline and early) [45].

Our results showed that radiomic models based on early and delta features performed better than the radiomic models based on baseline features. A possible explanation could be the fact that early and delta features consider the effect of the neoadjuvant CRT. These findings are consistent with our previous work on the role of radiomics on baseline PET imaging in patients with LACC treated with CRT followed by radical surgery, as radiomic features extracted from baseline scans on 195 patients could not predict histopathological tumour response and survival [22].

To our knowledge, this is the first study to investigate the role of early features and their variation from baseline (i.e., delta features) in the prediction of the outcome in terms of DFS and OS, in patients with LACC. Previously, Yang et al. explored the capacity of temporal intratumoural heterogeneity metrics to predict tumour response to therapy in LACC patients treated with exclusive CRT, showing that these features decreased significantly with time in responders [7]. Ho et al. showed that a combination of a pretreatment textural feature (grey level non-uniformity derived from GLSZM) and the temporal variation of total lesion glycolysis could

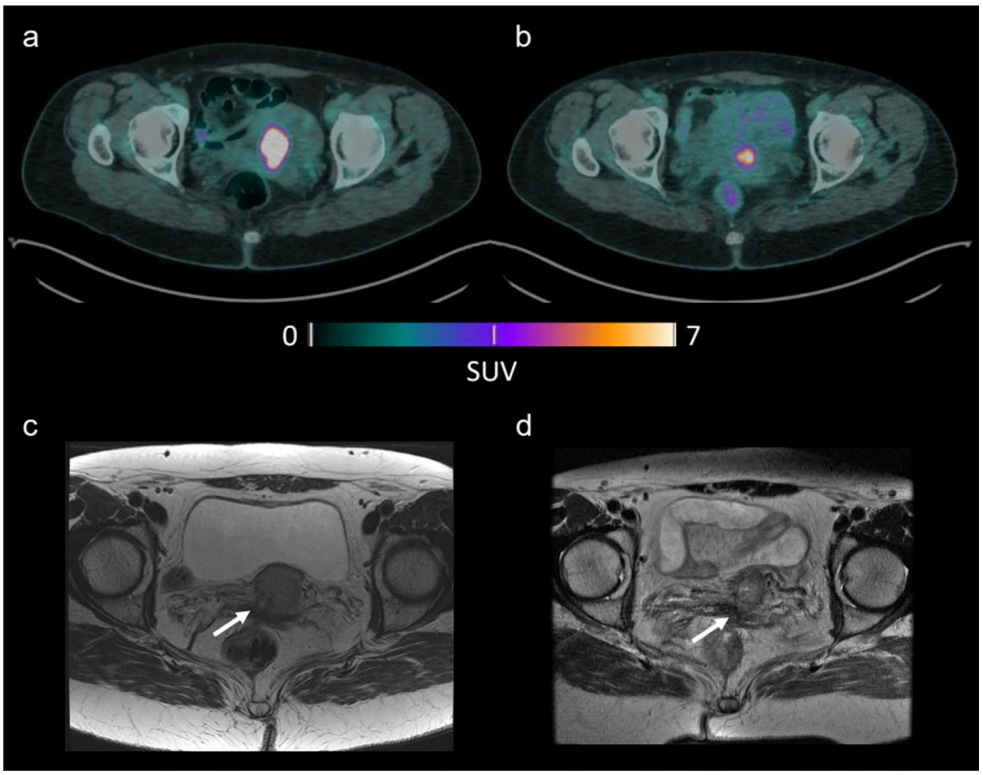


**Fig. 3** A 56-year-old woman with LACC. (**a**) Baseline [$^{18}$F]FDG PET/CT showing focal and intense [$^{18}$F]FDG uptake ($SUV_{max}$ 12.71, $SUV_{mean}$ 8.92, metabolic tumour volume (MTV) 10.69, total lesion glycolysis (TLG) 95.37); (**b**) early [$^{18}$F]FDG PET/CT showing reduced [$^{18}$F]FDG uptake ($SUV_{max}$ 6.31, $SUV_{mean}$ 4.33, MTV 39.69, TLG 171.70, delta-$SUV_{max}$ 50%, delta-$SUV_{mean}$ 52%, delta-MTV 63%, delta-TLG 82%) and reduced dimensions. (**c**) Baseline and (**d**) early MRI images, axial T2-weighted, showing the tumour (white arrow). Maximum tumour diameters on MRI: baseline, 3.7 cm; early, 2.1 cm. Histopathology after surgery showed complete response (pR0) and no pelvic lymph nodal involvement. The patient did not experience recurrence or death (follow-up time: 81.44 months)

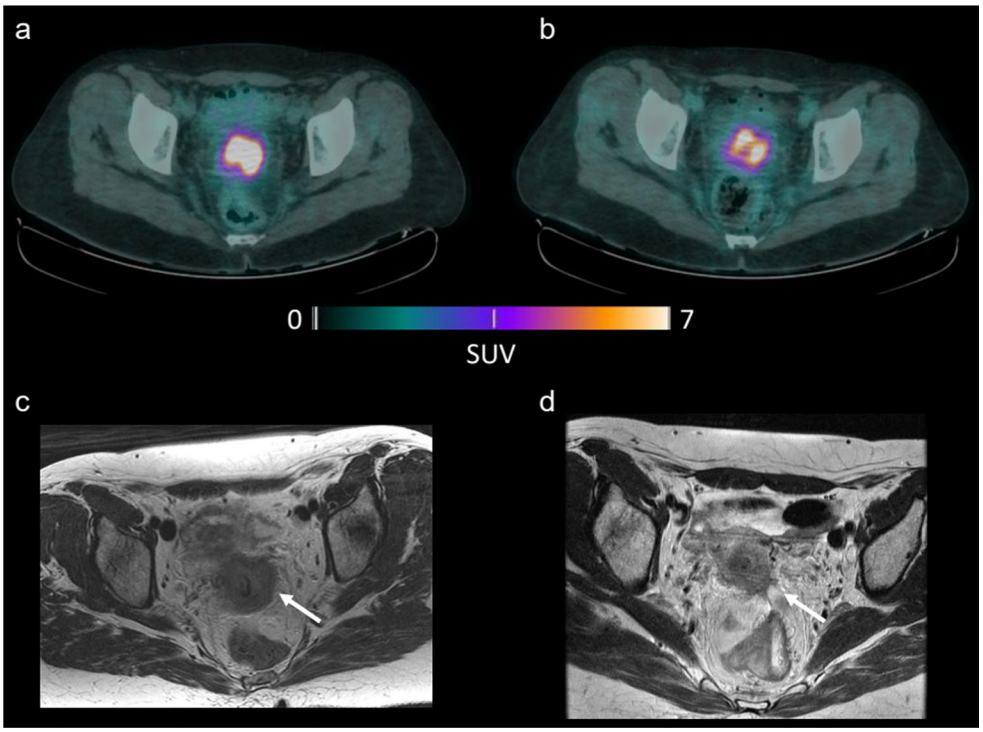


**Fig. 4** A 50-year-old woman with LACC. (**a**) Baseline [$^{18}$F]FDG PET/CT showing focal and intense [$^{18}$F]FDG uptake ($SUV_{max}$ 15.88, $SUV_{mean}$ 10.35, MTV 17.22, TLG 178.23); (**b**) early [$^{18}$F]FDG PET/CT showing heterogeneous [$^{18}$F]FDG uptake ($SUV_{max}$ 9.13, $SUV_{mean}$ 6.18, MTV 17.02, TLG 105.14, delta-$SUV_{max}$ 42%, delta-$SUV_{mean}$ 40%, delta-MTV 1%, delta-TLG 41%) (**c**) Baseline and (**d**) early MRI images, axial T2-weighted, showing the tumour (white arrow). Maximum tumour diameters on MRI: baseline, 4.8 cm; early, 2.1 cm. Histopathology after surgery showed partial response (pR2, 10 mm) and no pelvic nodal involvement. The patient experienced local recurrence after 19.88 months and died after 42.18 months

identify LACC patients with poor response to exclusive CRT [9]. However, we did not directly compare the results of our study to the previous ones, since standardization procedures, such as the IBSI [34], were not available at the time of these publications.

This study has several strengths. Firstly, the survival analysis has been conducted on a homogeneous population that has a long follow-up, with a median time of 76.0 months. Secondly, this is the first study on this topic where radiomic features were calculated using a software compliant with

**Table 2** Performances of the Cox proportional hazards model of the clinical, radiomic and combined model for prediction of disease-free survival (DFS) and overall survival (OS), expressed as mean C-Index of the testing cohorts' performances ($n = 19$)

| Timepoint | | DFS (C-index (95% CI)) | OS (C-index (95% CI)) |
|---|---|---|---|
| Baseline | Radiomic model | 0.51 (0.27–0.74) | 0.57 (0.31–0.83) |
| | Clinical model | 0.68 (0.47–0.88) | 0.76 (0.58–0.93) |
| | Combined model | 0.64 (0.41–0.87) | 0.76 (0.58–0.94) |
| Early | Radiomic model | 0.57 (0.34–0.80) | 0.75 (0.52–0.98) |
| | Clinical model | 0.68 (0.47–0.88) | 0.76 (0.58–0.93) |
| | Combined model | 0.70 (0.50–0.90) | 0.75 (0.54–0.97) |
| Delta | Radiomic model | 0.66 (0.45–0.88) | 0.79 (0.60–0.97) |
| | Clinical model | 0.68 (0.47–0.88) | 0.76 (0.58–0.93) |
| | Combined model | 0.72 (0.52–0.93) | 0.78 (0.57–0.98) |

*DFS* disease-free survival. *CI* confidence interval. *OS* overall survival

**Table 3** Selected features for the radiomic models

| Outcome | Timepoint | Feature (feature family) |
|---|---|---|
| DFS | Baseline | Geary's C (shape)<br>Asphericity (shape)<br>Kurtosis (statistics, intensity histogram) |
| | Early | Dependence count energy (texture, 3D merged NGLDM feature)<br>Major axis length (shape)<br>Grey level non-uniformity (texture, 3D GLDZM feature)<br>Least axis length (shape) |
| | Delta | Kurtosis (statistics, intensity histogram)<br>Zone size entropy (texture, 3D GLSZM feature)<br>Intensity fraction difference between volume fractions (statistics, intensity-volume histogram) |
| OS | Baseline | Geary's C (shape)<br>Kurtosis (statistics, intensity histogram)<br>Moran's I (shape) |
| | Early | Least axis length (shape)<br>Dependence count energy (texture, 3D merged NGLDM feature)<br>Information correlation 2 (texture, 3D merged GLCM feature) |
| | Delta | Minor axis length (shape)<br>Least axis length (shape)<br>Cluster shade (texture, 3D merged GLCM feature)<br>Area density AABB (shape) |

*DFS* Disease-free survival. *NGLDM* Neighbouring grey level dependence matrix. *GLDZM* Grey level distance zone matrix. *GLSZM* Grey level size zone matrix. *OS* Overall survival. *GLCM* Grey level co-occurrence matrix. *AABB* Axis-aligned bounding box

the IBSI guidelines, which ensures statistical reliability and repeatability of the results [33, 34]. Moreover, to ensure the reproducibility of the results, we have internally validated the model with a stratified 5-folds cross-validation.

The study has also some limitations: one of the main weaknesses is that this study has been conducted retrospectively in a single centre, like most radiomic studies [7, 8, 10–14, 18, 20]. We are aware that exclusive CRT is currently the standard of care for LACC patients [1], however, no differences in survival outcomes have been reported in a large, randomized trial comparing exclusive CRT with neoadjuvant CRT followed by surgery [4].We included patients with different tumour histotype (i.e., squamous cell and adenocarcinomas). Squamous and adenocarcinomas have different prognosis, but when comparing two different timepoints we are focusing on the same histotype. We chose to include both tumour types to be representative of the most frequent histotypes in LACC and evaluate the usefulness of radiomics in a real-life setting. A semiautomated segmentation method was used to delineate the primary tumours; however, due to the proximity of the cervix uteri to areas of physiological high [$^{18}$F]FDG activity (e.g., bladder, ureters) and the small size of the lesions (especially in the early imaging), manual correction was applied in one third of the VOIs. These unavoidable manual adjustments, although supervised by two experienced—but different—observers, may have introduced inter-observer variability in the measurements. Future prospective studies should consider the use of a urinary catheter to empty the bladder to improve tumour visualization by reducing [$^{18}$F]FDG accumulation in the region surrounding the tumour. Lastly, PET/CT images were acquired using two different PET/CT scanners, with an unbalanced ratio of patients acquired on Gemini GXL and Biograph mCT (83% vs. 17% of the overall scans, respectively), which could have precluded a robust normalization of the data. However, all images were acquired and reconstructed according to EANM guidelines [27] and EARL $^{18}$F standard 1 [28], respectively, that has been reported to produce a wide range of reliable, repeatable, and reproducible radiomic features [43]. An alternative approach could have been using the ComBat method to harmonize the radiomic features; however, this was not feasible due to the limited number of scans acquired on the Siemens scanner [46]. For future research, deep learning-based harmonization techniques could be also used to minimise variations between different scanners [47].

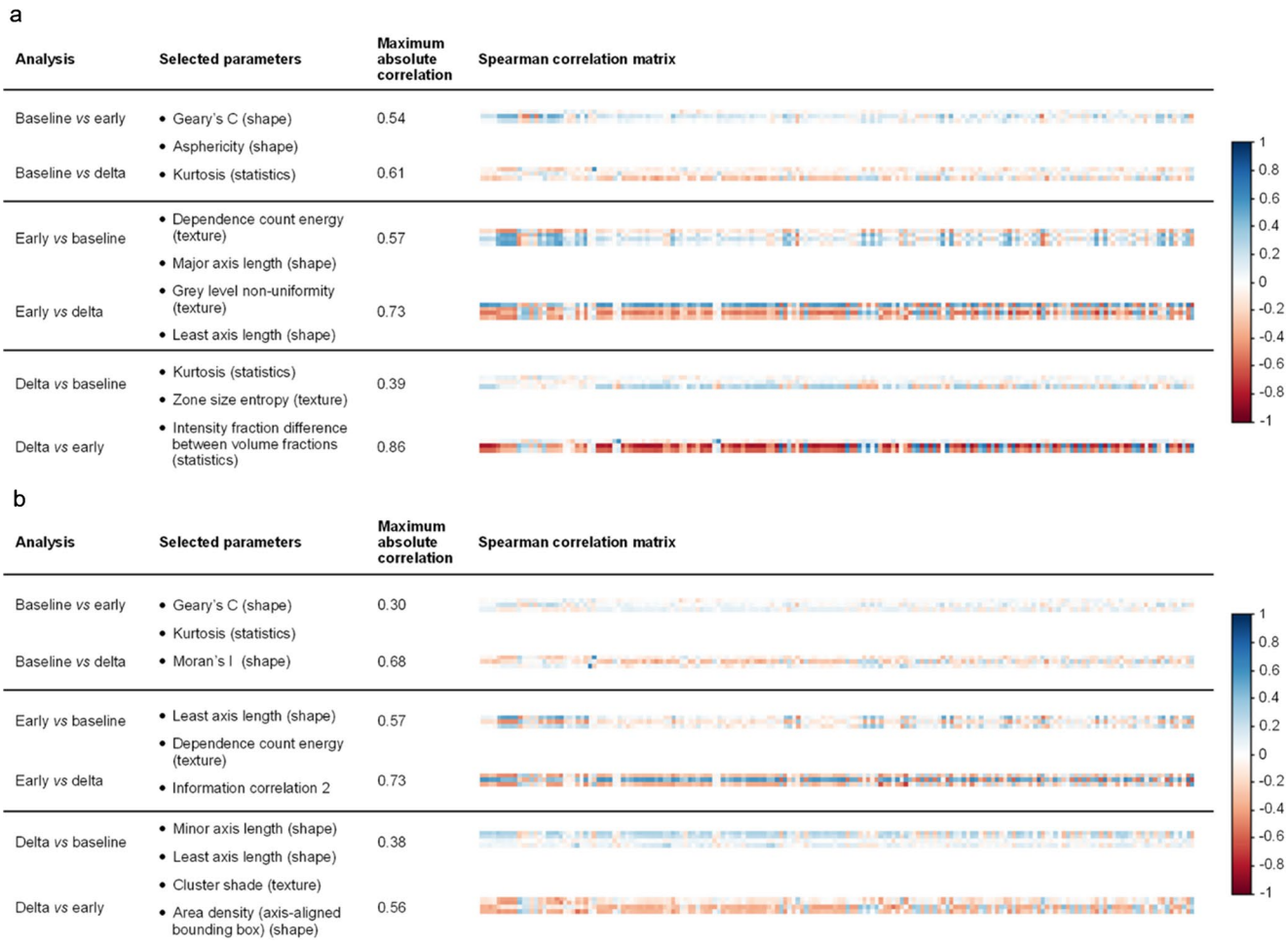


**Fig. 5** Heatmaps of the Spearman correlation matrix of the relation between the selected features for each timepoint vs. the features of the remaining two timepoints, for the two outcomes (A, disease-free survival, and B, overall survival)

## Conclusions

In this study, [$^{18}$F]FDG-PET early and delta radiomic features could not predict DFS in patients with LACC treated with neoadjuvant CRT followed by surgery. Although slightly improved performances for the radiomic and combined models were observed in the prediction of OS compared to the clinical model, the added value of these information seems to be limited, compared to the challenging process of feature extraction.

**Supplementary Information** The online version contains supplementary material available at https://doi.org/10.1007/s00259-025-07405-w.

**Acknowledgements** We thank Marco De Summa, M.Sc., for his help with data collection.

**Authors contribution** All authors contributed to the study conception and design. Material preparation, data collection and analysis were performed by A.F., W.A.N., N.B., T.P., V.F., F.H.P.v.V., and A.C. The first draft of the manuscript was written by A.F., and all authors commented on previous versions of the manuscript. All authors read and approved the final manuscript.

**Funding** This study was supported by a Short-term Fellowship (2022) granted to Anita Florit by Fondazione AIRC (Associazione Italiana per la Ricerca sul Cancro) and by an internal university grant (Università Cattolica Line D.1 2024-R4124501519) to Vittoria Rufini. No potential conflict of interest relevant to this article was reported.

**Data availability** The datasets generated during and/or analysed during the current study are available from the corresponding author on reasonable request.

**Ethics and consent to participate** Informed consent was obtained from all individual participants included in the study.

**Financial interests** The authors have no financial or proprietary interests in any material discussed in this article.

## References

1. NCCN Clinical Practice Guidelines in Oncology (NCCN guidelines) for Cervical cancer V.4.2025. National Comprehensive

Cancer Network, Inc. 2025. https://www.nccn.org/professionals/physician_gls/pdf/cervical.pdf. Accessed 4 June 2025.
2. Quinn MA, Benedet JL, Odicino F, Maisonneuve P, Beller U, Creasman WT, et al. Carcinoma of the cervix Uteri. Int J Gynaecol Obstet. 2006;95:S43–103. https://doi.org/10.1016/S0020-7292(06)60030-1.
3. Espenel S, Garcia MA, Trone JC, Guillaume E, Harris A, Rehailia-Blanchard A, et al. From IB2 to IIIB locally advanced cervical cancers: report of a ten-year experience. Radiat Oncol. 2018;13(1):16. https://doi.org/10.1186/s13014-018-0963-8.
4. Cetina L, González-Enciso A, Cantú D, Coronel J, Pérez-Montiel D, Hinojosa J, et al. Brachytherapy versus radical hysterectomy after external beam chemoradiation with gemcitabine plus cisplatin: a randomized, phase III study in IB2-IIB cervical cancer patients. Ann Oncol. 2013;24:2043–7. https://doi.org/10.1093/annonc/mdt142.
5. Lambin P, Rios-Velazquez E, Leijenaar R, Carvalho S, van Stiphout RGPM, Granton P, et al. Radiomics: extracting more information from medical images using advanced feature analysis. Eur J Cancer. 2012;48:441–6. https://doi.org/10.1016/j.ejca.2011.11.036.
6. Hatt M, Tixier F, Pierce L, Kinahan PE, Le Rest CC, Visvikis D. Characterization of PET/CT images using texture analysis: the past, the present… any future? Eur J Nucl Med Mol Imaging. 2017;44:151–65. https://doi.org/10.1007/s00259-016-3427-0.
7. Yang F, Thomas MA, Dehdashti F, Grigsby PW. Temporal analysis of intratumoral metabolic heterogeneity characterized by textural features in cervical cancer. Eur J Nucl Med Mol Imaging. 2013;40:716–27. https://doi.org/10.1007/s00259-012-2332-4.
8. Yang F, Young L, Grigsby P. Predictive value of standardized intratumoral metabolic heterogeneity in locally advanced cervical Cancer treated with chemoradiation. Int J Gynecol Cancer. 2016;26:777–84. https://doi.org/10.1097/igc.0000000000000616.
9. Ho K-C, Fang Y-HD, Chung H-W, Yen T-C, Ho T-Y, Chou H-H, et al. A preliminary investigation into textural features of intratumoral metabolic heterogeneity in (18)F-FDG PET for overall survival prognosis in patients with bulky cervical cancer treated with definitive concurrent chemoradiotherapy. Am J Nucl Med Mol Imaging. 2016;6:166–75.
10. Reuzé S, Orlhac F, Chargari C, Nioche C, Limkin E, Riet F, et al. Prediction of cervical cancer recurrence using textural features extracted from $^{18}$F-FDG PET images acquired with different scanners. Oncotarget. 2017;8:43169–79. https://doi.org/10.18632/oncotarget.17856.
11. Altazi BA, Fernandez DC, Zhang GG, Hawkins S, Naqvi SM, Kim Y, et al. Investigating multi-radiomic models for enhancing prediction power of cervical cancer treatment outcomes. Phys Med. 2018;46:180–8. https://doi.org/10.1016/j.ejmp.2017.10.009.
12. Chen S-W, Shen W-C, Hsieh T-C, Liang J-A, Hung Y-C, Yeh L-S, et al. Textural features of cervical cancers on FDG-PET/CT associate with survival and local relapse in patients treated with definitive chemoradiotherapy. Sci Rep. 2018;8:11859. https://doi.org/10.1038/s41598-018-30336-6.
13. Schernberg A, Reuze S, Orlhac F, Buvat I, Dercle L, Sun R, et al. A score combining baseline neutrophilia and primary tumor SUVpeak measured from FDG PET is associated with outcome in locally advanced cervical cancer. Eur J Nucl Med Mol Imaging. 2018;45:187–95. https://doi.org/10.1007/s00259-017-3824-z.
14. Lucia F, Visvikis D, Desseroit M-C, Miranda O, Malhaire J-P, Robin P, et al. Prediction of outcome using pretreatment $^{18}$F-FDG PET/CT and MRI radiomics in locally advanced cervical cancer treated with chemoradiotherapy. Eur J Nucl Med Mol Imaging. 2018;45:768–86. https://doi.org/10.1007/s00259-017-3898-7.
15. Lucia F, Visvikis D, Vallières M, Desseroit M-C, Miranda O, Robin P, et al. External validation of a combined PET and MRI radiomics model for prediction of recurrence in cervical cancer patients treated with chemoradiotherapy. Eur J Nucl Med Mol Imaging. 2019;46:864–77. https://doi.org/10.1007/s00259-018-4231-9.
16. Mu W, Liang Y, Hall LO, Tan Y, Balagurunathan Y, Wenham R, et al. $^{18}$F-FDG PET/CT habitat radiomics predicts outcome of patients with cervical Cancer treated with chemoradiotherapy. Radiol Artif Intell. 2020;2:e190218. https://doi.org/10.1148/ryai.2020190218.
17. Ferreira M, Lovinfosse P, Hermesse J, Decuypere M, Rousseau C, Lucia F, et al. [$^{18}$F]FDG PET radiomics to predict disease-free survival in cervical cancer: a multi-scanner/center study with external validation. Eur J Nucl Med Mol Imaging. 2021;48:3432–43. https://doi.org/10.1007/s00259-021-05303-5.
18. de Alencar NRG, Machado MAD, Mourato FA, de Oliveira ML, Moraes TF, Mattos Junior LAR, et al. Exploratory analysis of radiomic as prognostic biomarkers in $^{18}$F-FDG PET/CT scan in uterine cervical cancer. Front Med (Lausanne). 2022;9:1046551. https://doi.org/10.3389/fmed.2022.1046551.
19. Cho H-W, Lee ES, Lee JK, Eo JS, Kim S, Hong JH. Prognostic value of textural features obtained from F-fluorodeoxyglucose (F-18 FDG) positron emission tomography/computed tomography (PET/CT) in patients with locally advanced cervical cancer undergoing concurrent chemoradiotherapy. Ann Nucl Med. 2023;37:44–51. https://doi.org/10.1007/s12149-022-01802-z.
20. Liu H, Cui Y, Chang C, Zhou Z, Zhang Y, Ma C, et al. Development and validation of a $^{18}$F-FDG PET/CT radiomics nomogram for predicting progression free survival in locally advanced cervical cancer: a retrospective multicenter study. BMC Cancer. 2024;24:150. https://doi.org/10.1186/s12885-024-11917-3.
21. Bhatla N, Berek JS, Cuello Fredes M, Denny LA, Grenman S, Karunaratne K, et al. Revised FIGO staging for carcinoma of the cervix Uteri. Int J Gynaecol Obstet. 2019;145:129–35. https://doi.org/10.1002/ijgo.12749.
22. Collarino A, Feudo V, Pasciuto T, Florit A, Pfaehler E, de Summa M, et al. Is PET radiomics useful to predict pathologic tumor response and prognosis in locally advanced cervical cancer? J Nucl Med. 2024;65(6):962–70. https://doi.org/10.2967/jnumed.123.267044
23. Harris PA, Taylor R, Thielke R, Payne J, Gonzalez N, Conde JG. Research electronic data capture (REDCap)—a metadata-driven methodology and workflow process for providing translational research informatics support. J Biomed Inf. 2009;42:377–81. https://doi.org/10.1016/j.jbi.2008.08.010.
24. Ferrandina G, Gambacorta A, Gallotta V, Smaniotto D, Fagotti A, Tagliaferri L, et al. Chemoradiation with concomitant boosts followed by radical surgery in locally advanced cervical cancer: long-term results of the ROMA-2 prospective phase 2 study. Int J Radiat Oncol Biol Phys. 2014;90:778–85. https://doi.org/10.1016/j.ijrobp.2014.07.033.
25. Zannoni GF, Vellone VG, Carbone A. Morphological effects of radiochemotherapy on cervical carcinoma: a morphological study of 50 cases of hysterectomy specimens after neoadjuvant treatment. Int J Gynecol Pathol. 2008;27:274–81. https://doi.org/10.1097/pgp.0b013e31815b1263.
26. Rufini V, Collarino A, Calcagni ML, Meduri GM, Fuoco V, Pasciuto T, et al. The role of 18F-FDG-PET/CT in predicting the histopathological response in locally advanced cervical carcinoma treated by chemo-radiotherapy followed by radical surgery: a prospective study. Eur J Nucl Med Mol Imaging. 2020;47:1228–38. https://doi.org/10.1007/s00259-019-04436-y.
27. Boellaard R, Delgado-Bolton R, Oyen WJG, Giammarile F, Tatsch K, Eschner W, et al. FDG PET/CT: EANM procedure guidelines for tumour imaging: version 2.0. Eur J Nucl Med Mol

Imaging. 2015;42:328–54. https://doi.org/10.1007/s00259-014-2961-x.
28. Kaalep A, Sera T, Oyen W, Krause BJ, Chiti A, Liu Y, et al. EANM/EARL FDG-PET/CT accreditation - summary results from the first 200 accredited imaging systems. Eur J Nucl Med Mol Imaging. 2018;45:412–22. https://doi.org/10.1007/s00259-017-3853-7.
29. Boellaard R. Quantitative oncology molecular analysis suite: ACCURATE. J Nucl Med. 2018;59:1753.
30. Frings V, van Velden FHP, Velasquez LM, Hayes W, van de Ven PM, Hoekstra OS, et al. Repeatability of metabolically active tumor volume measurements with FDG PET/CT in advanced Gastrointestinal malignancies: a multicenter study. Radiology. 2014;273:539–48. https://doi.org/10.1148/radiol.14132807.
31. Collarino A, Garganese G, Fragomeni SM, Pereira Arias-Bouda LM, Ieria FP, Boellaard R, et al. Radiomics in vulvar cancer: first clinical experience using $^{18}$F-FDG PET/CT images. J Nucl Med. 2019;60:199–206. https://doi.org/10.2967/jnumed.118.215889.
32. Pfaehler E, Mesotten L, Zhovannik I, Pieplenbosch S, Thomeer M, Vanhove K, et al. Plausibility and redundancy analysis to select FDG-PET textural features in non-small cell lung cancer. Med Phys. 2021;48:1226–38. https://doi.org/10.1002/mp.14684.
33. Pfaehler E, Zwanenburg A, de Jong JR, Boellaard R, RaCaT. An open source and easy to use radiomics calculator tool. PLoS ONE. 2019;14:e0212223. https://doi.org/10.1371/journal.pone.0212223.
34. Zwanenburg A, Vallières M, Abdalah MA, Aerts HJWL, Andrearczyk V, Apte A, et al. The image biomarker standardization initiative: standardized quantitative radiomics for High-Throughput image-based phenotyping. Radiology. 2020;295:328–38. https://doi.org/10.1148/radiol.2020191145.
35. van Timmeren JE, Carvalho S, Leijenaar RTH, Troost EGC, van Elmpt W, de Ruysscher D, et al. Challenges and caveats of a multi-center retrospective radiomics study: an example of early treatment response assessment for NSCLC patients using FDG-PET/CT radiomics. PLoS ONE. 2019;14:e0217536. https://doi.org/10.1371/journal.pone.0217536.
36. Cox DR. Regression models and Life-Tables. J R Stat Soc Ser B Stat Methodol. 1972;34:187–202.
37. R Core Team (2025) R: a language and environment for statistical computing. R Foundation for Statistical Computing, Vienna, Austria. https://www.R-project.org/
38. Peeters CFW, Übelhör C, Mes SW et al. Stable prediction with radiomics data. 2019. https://doi.org/10.48550/arXiv.1903.11696
39. Ishwaran H, Kogalur UB, Blackstone EH, Lauer MS. Random survival forests. Ann Appl Stat. 2008;2:841–60. https://doi.org/10.1214/08-AOAS169.
40. Amini M, Hajianfar G, Hadadi Avval A, Nazari M, Deevband MR, Oveisi M, et al. Overall survival prognostic modelling of Non-small cell lung Cancer patients using positron emission tomography/computed tomography harmonised radiomics features: the quest for the optimal machine learning algorithm. Clin Oncol (R Coll Radiol). 2022;34:114–27. https://doi.org/10.1016/j.clon.2021.11.014.
41. Harrell FE Jr, Califf RM, Pryor DB, Lee KL, Rosati RA. Evaluating the yield of medical tests. JAMA. 1982;247:2543–6.
42. Demircioğlu A. The effect of data resampling methods in radiomics. Sci Rep. 2024;14:2858. https://doi.org/10.1038/s41598-024-53491-5.
43. Pfaehler E, van Sluis J, Merema BBJ, van Ooijen P, Berendsen RCM, van Velden FHP, et al. Experimental multicenter and multivendor evaluation of the performance of PET radiomic features using 3-Dimensionally printed Phantom inserts. J Nucl Med. 2020;61:469–76. https://doi.org/10.2967/jnumed.119.229724.
44. Hatt M, Majdoub M, Vallières M, Tixier F, Le Rest CC, Groheux D, et al. $^{18}$F-FDG PET uptake characterization through texture analysis: investigating the complementary nature of heterogeneity and functional tumor volume in a multi-cancer site patient cohort. J Nucl Med. 2015;56:38–44. https://doi.org/10.2967/jnumed.114.144055.
45. Mansor S, Pfaehler E, Heijtel D, Lodge MA, Boellaard R, Yaqub M. Impact of PET/CT system, reconstruction protocol, data analysis method, and repositioning on PET/CT precision: an experimental evaluation using an oncology and brain Phantom. Med Phys. 2017;44:6413–24. https://doi.org/10.1002/mp.12623.
46. Orlhac F, Eertink JJ, Cottereau A-S, Zijlstra JM, Thieblemont C, Meignan M, et al. A guide to combat harmonization of imaging biomarkers in multicenter studies. J Nucl Med. 2022;63:172–9. https://doi.org/10.2967/jnumed.121.262464.
47. Haberl D, Spielvogel CP, Jiang Z, Orlhac F, Iommi D, Carrió I, et al. Multicenter PET image harmonization using generative adversarial networks. Eur J Nucl Med Mol Imaging. 2024;51(9):2532–46. https://doi.org/10.1007/s00259-024-06708-8.

## Authors and Affiliations

**Anita Florit[1,2] · Wyanne A. Noortman[3] · Nicolò Bizzarri[4] · Tina Pasciuto[5,6] · Vanessa Feudo[7] · Salvatore Annunziata[1] · Lioe-Fee de Geus-Oei[2,8,9] · Elisabeth Pfaehler[10] · Ronald Boellaard[11] · Maria Antonietta Gambacorta[12,13] · Gian Franco Zannoni[14,15] · Gabriella Ferrandina[4,16] · Evis Sala[13,17] · Giovanni Scambia[4,16] · Vittoria Rufini[1,7] · Floris H. P. van Velden[8] · Angela Collarino[1]**

✉ Vittoria Rufini
vittoria.rufini@unicatt.it

Anita Florit
anita.florit@guest.policlinicogemelli.it

1 Nuclear Medicine Unit, Department of Diagnostic Imaging and Oncological Radiotherapy, Fondazione Policlinico Universitario A. Gemelli IRCCS, Largo A. Gemelli, 8, 00168 Rome, Italy

2 Biomedical Photonic Imaging Group, University of Twente, Enschede, The Netherlands

3 Department of Medical Oncology, University Medical Center Groningen, Groningen, The Netherlands

4 Gynaecologic Oncology Unit, Department of Women, Children and Public Health Sciences, Fondazione Policlinico Universitario A. Gemelli IRCCS, Rome, Italy

5 Research Core Facility Data Collection G-STeP, Fondazione Policlinico Universitario A. Gemelli IRCCS, Rome, Italy

6 Section of Hygiene, University Department of Life Sciences and Public Health, Università Cattolica del Sacro Cuore, Rome, Italy

7 Section of Nuclear Medicine, University Department of Radiological Sciences and Haematology, Università Cattolica del Sacro Cuore, Rome, Italy

8 Section of Nuclear Medicine, Department of Radiology, Leiden University Medical Center, Leiden, The Netherlands

9 Department of Radiation Science and Technology, Delft University of Technology, Delft, The Netherlands

10 Institute of Neuroscience and Medicine, INM-4, Forschungszentrum Jülich GmbH, Jülich, Germany

11 Department of Radiology and Nuclear Medicine, Amsterdam UMC, Location VU University Medical Center, Amsterdam, The Netherlands

12 Radiation Oncology Unit, Department of Diagnostic Imaging and Oncological Radiotherapy, Fondazione Policlinico Universitario A. Gemelli IRCCS, Rome, Italy

13 Section of Radiology, University Department of Radiological Sciences and Haematology, Università Cattolica del Sacro Cuore, Rome, Italy

14 Gynaecopathology Unit, Department of Women, Children and Public Health Sciences, Fondazione Policlinico Universitario A. Gemelli IRCCS, Rome, Italy

15 Section of Pathology, University Department of Life Sciences and Public Health, Università Cattolica del Sacro Cuore, Rome, Italy

16 Section of Obstetrics and Gynaecology, University Department of Life Sciences and Public Health, Università Cattolica del Sacro Cuore, Rome, Italy

17 Advanced Radiodiagnostics Centre, Department of Diagnostic Imaging and Oncological Radiotherapy, Fondazione Policlinico Universitario A. Gemelli IRCCS, Rome, Italy